Pressure effect on the magnetism of the diluted magnetic semiconductor $(Ba_{1-x}K_x)(Zn_{1-y}Mn_y)_2As_2$ with independent spin and charge doping

F. Sun,[1,2,3] N. N. Li,[2] B. J. Chen,[1] Y. T. Jia,[1] L. J. Zhang,[2] W. M. Li,[1] G. Q. Zhao,[1] L. Y. Xing,[1] G. Fabbris,[3,4] Y. G. Wang,[5] Z. Deng,[1] Y. J. Uemura,[6] H. K. Mao,[2,5] D. Haskel,[3,*] W. G. Yang,[2,5,*] and C. Q. Jin[1,7,*]

[1]*Beijing National Laboratory for Condensed Matter Physics and Institute of Physics, Chinese Academy of Sciences, Beijing 100190, China*

[2]*Center for High Pressure Science & Technology Advanced Research (HPSTAR), Shanghai, 201203, China*

[3]*Advanced Photon Source (APS), Argonne National Laboratory, Argonne, Illinois 60439, USA*

[4]*Department of Physics, Washington University, St. Louis, Missouri 63130, USA*

[5]*High Pressure Synergetic Consortium (HPSynC), Geophysical Laboratory, Carnegie Institution of Washington, Argonne, Illinois 60439, USA*

[6]*Department of Physics, Columbia University, New York, New York 10027, USA*

[7]*Collaborative Innovation Center of Quantum Matter, Beijing 100871, China*

(Received 18 March 2016; revised manuscript received 11 May 2016; published 3 June 2016)

We used x-ray magnetic circular dichroism (XMCD) to probe the ferromagnetic properties of As p-symmetric ($4p$) states in the recently synthesized diluted magnetic semiconductor $(Ba_{1-x}K_x)(Zn_{1-y}Mn_y)_2As_2$ system under ambient- and high-pressure conditions. The As K-edge XMCD signal scales with the sample magnetization (dominated by Mn) and scales with the ferromagnetic ordering temperature Tc, and hence it is representative of the bulk magnetization. The XMCD intensity gradually decreases upon compression and vanishes at around 25 GPa, indicating quenching of ferromagnetism at this pressure. Transport measurements show a concomitant increase in conductivity with pressure, leading to a nearly metallic state at about the same pressure where magnetic order collapses. High-pressure x-ray diffraction shows an absence of structural transitions to 40 GPa. The results indicate that the mobility of doped holes, probed by both transport and x-ray absorption spectroscopy ($4p$ band broadening), is intimately connected with the mechanism of magnetic ordering in this class of compounds and that its control using external pressure provides an alternative route for tuning the magnetic properties in diluted magnetic semiconductor materials.

DOI: 10.1103/PhysRevB.93.224403

I. INTRODUCTION

Diluted magnetic semiconductor (DMS) materials, combining the tunability of charge and spin degrees of freedom, offer a rich variety of remarkable properties that attract extensive interest in materials science as well as opening prospects for the design of new functional spintronic devices [1–5]. Rapid progress on DMS research started in the 1990s, to a large extent, owing to the development of crystal growth methods far from thermal equilibrium, especially by molecular beam epitaxy (MBE) techniques. In the Mn-doped III–V DMS systems, Mn substituting for the trivalent cation (Ga) is simultaneously an acceptor and a source of magnetic moments. This dual role of Mn presents an obstacle to both material synthesis and theoretical understanding. The recently discovered Mn-doped I-II-V semiconductor $Li_{1+x}(Zn_{1-y}Mn_y)As$ [6] and Mn-doped II-II-V semiconductor $(Ba_{1-x}K_x)(Zn_{1-y}Mn_y)_2As_2$ [7], belonging to a new generation of bulk ferromagnets, exhibit certain advantages over the (III, Mn)V–based materials. Key differences exist between these new types of DMS and (III, Mn)V materials like (Ga, Mn)As in both the mechanism of spin and charge injection and the intricacies of material synthesis. In semiconductor $(Ba_{1-x}K_x)(Zn_{1-y}Mn_y)_2As_2$, holes are induced by (Ba^{2+},K^{1+}) replacement independent of spin doping, which is induced via (Zn^{2+},Mn^{2+}) replacement. Bulk samples display ferromagnetic ordering with Curie temperature, Tc, up to 230 K [8], which has been significantly enhanced from Tc $\sim$ 50 K of $Li_{1+x}(Zn_{1-y}Mn_y)As$ and is higher than the highest Tc $\sim$ 200 K for (Ga, Mn)As [9].

The physical properties of DMS materials are strongly sensitive to external factors such as magnetic field, temperature, and pressure. In addition to the crystal structure, the magnetism plays a key role in determining the physical properties. Therefore, a key route to obtaining further insight on the underlying mechanism leading to magnetic order in DMS materials is via control of the ferromagnetic response with tunable thermodynamic conditions. In this context, external pressure offers interesting opportunities [10], because it can modify both electronic bandwidths and band gaps in DMSs without introducing chemical disorder inherent to doping, and therefore it is an effective method to draw out the complicated interplay among structural, magnetic, and electronic degrees of freedom in these novel ferromagnets.

Recent theory [11] of Mn-doped II-II-V semiconductors, e.g., $(Ba_{1-x}K_x)(Zn_{1-y}Mn_y)_2As_2$, predicts that the magnetic ordering emerges from the competition between the short-range antiferromagnetic (superexchange) interaction and a longer-range ferromagnetic interaction mediated by the itinerant As holes. This model also predicts an induced magnetic moment on As atoms that couples antiparallel to the Mn $3d$ moments. The general understanding for most common (III, Mn)V–based DMSs invokes As-derived valence-band states [12,13] as mediators of ferromagnetic interactions. However, for the new-generation Mn-doped II-II-V semiconductors, the details of the electronic band structure and the role of As mediating (hole) states remain unresolved both in

*Corresponding authors: haskel@aps.anl.gov; yangwg@hpstar.ac.cn; jin@iphy.ac.cn

experiment and theory. Thus, it is necessary to get in-depth insight into the role of As valence-band states to verify the theory of carrier-mediated long-range ferromagnetic order and to identify the nature of the mediating states.

The combination of hard x-ray magnetic circular dichroism (XMCD) and diamond anvil cell techniques has proven to be a valuable way to study stability of ferromagnetism to applied pressure [14–18]. In this paper, we report the pressure effect on the electronic properties of $(Ba_{1-x}K_x)(Zn_{1-y}Mn_y)_2As_2$ using XMCD at the As *K*-edge. XMCD is the difference in x-ray absorption (XAS) measured with right (μ^+) and left (μ^-) circularly polarized photons. The transfer of photon angular momentum to the excited photoelectron allows the orbital magnetization of the *p*-symmetric ($4p$) states to be probed. The *K*-edge XMCD signal of first-row transition metal atoms Fe, Co, and Ni [19–21], as well as Mn in (Ga, Mn)As and (In, Mn)As [22,23], arises from polarization of $4p$ orbitals induced by $4p$-$3d$ hybridization with $3d$ orbitals of neighboring magnetic sites. This hybridization is also the source of As $4p$ polarization in our Mn-doped II-II-V DMS samples, probed by XMCD at the As *K*-edge.

II. RESULTS AND DISCUSSION

Polycrystalline $(Ba_{1-x}K_x)(Zn_{1-y}Mn_y)_2As_2$ samples were synthesized using the arc-melting solid state reaction method [7] and ground into fine powder before experiment. The samples were mounted on tapes for low-temperature experiments under ambient-pressure condition. For the high-pressure measurements, the sample was mixed with silicon oil and loaded into the diamond anvil cell together with Ruby markers for online pressure calibration at low temperature. A cryogenic superconducting magnet with a bore large enough to accommodate a membrane-driven CuBe diamond anvil cell (DAC) was used, allowing application of high fields (up to 6.5 T) and *in situ* control of pressure. The sample was cooled to ~2 K with He vapor. The XAS and XMCD measurements were conducted at beamline 4 ID-D of the Advanced Photon Source (APS) at Argonne National Laboratory. This hard x-ray beamline uses a diamond phase retarder to convert the incoming beam polarization from linear to circular. To obtain the XMCD signal, x-ray helicity was modulated at 13.1 Hz, and XMCD was detected with a lock-in amplifier. Ambient- and high-pressure XMCD data were collected with a magnetic field of 4 T and 2 T, respectively. Scans were repeated with opposite applied field direction to ensure artifact-free XMCD signals.

Figure 1 shows ambient pressure XAS and XMCD As *K*-edge spectra for $(Ba_{1-x}K_x)(Zn_{1-y}Mn_y)_2As_2$ samples with various hole and spin doping levels ($x = 0.25$, $y = 0.15$; $x = 0.25$, $y = 0.05$; $x = 0.10$, $y = 0.05$). The XMCD line shape and position relative to the absorption threshold [Fig. 1(a)] are consistent with those reported previously for (Ga, Mn)As ferromagnetic semiconductors [23], in which the dichroism signal consists of a single positive peak located at the low-energy side of the *K* absorption edge. The positive sign of the XMCD signal indicates that the induced As orbital moment is antiparallel to the total moment [24], which is dominated by the Mn $3d$ spin moment. Due to the electric dipole selection rules and the Pauli exclusion principle, an absorption spectrum

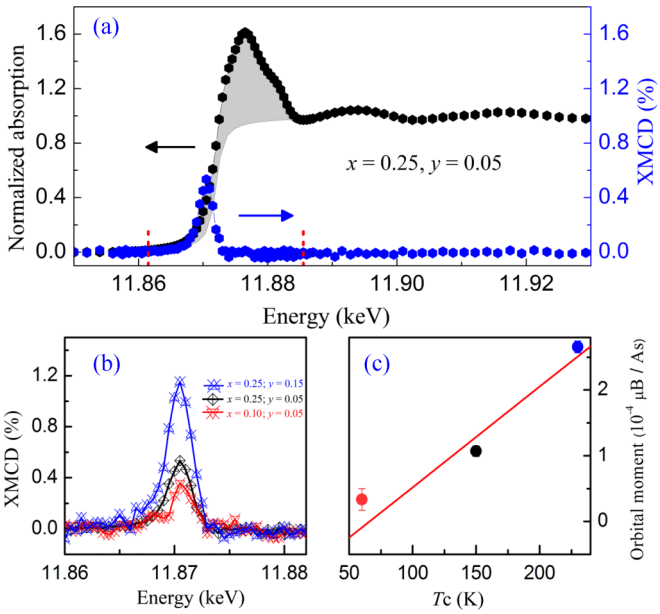

FIG. 1. (a) As *K*-edge x-ray absorption near edge structure (black curve) and XMCD (blue curve) data taken for $(Ba_{0.75}K_{0.25})(Zn_{0.95}Mn_{0.05})_2As_2$ at $T = 2$ K, $P = 1$ bar. Red dashed lines show the XAS and XMCD integrated range that was used in the sum rule. (b) XMCD spectra for $x = 0.25$, $y = 0.15$; $x = 0.25$, $y = 0.05$; $x = 0.10$, $y = 0.05$ compositions at $T = 2$ K, $P = 1$ bar. (c) Orbital magnetic moment per As ion vs Curie temperature *T*c for the same series of compositions.

from any state of the ground configuration l^n of the ion to any state of the final configuration cl^{n+1} (c denotes a core hole) is determined by the partial densities of unoccupied states with l character and their corresponding transition probabilities. The occurrence of an XMCD signal at the lower-energy side of the absorption edge indicates that the hole carriers introduced by K doping at Ba sites required for ferromagnetism reside on As $4p$ states near the valence-band edge. The doped charge (hole) carriers lead to a downward shift of the Fermi-level, E_f, which results in unoccupied states near E_f with As $4p$ character. To study the relationship between the As XMCD and the ferromagnetic ordering temperature *T*c, we measured XMCD spectra of $(Ba_{1-x}K_x)(Zn_{1-y}Mn_y)_2As_2$ with different doping levels under the same conditions ($H = 4$ T, $T = 2$ K), as shown in Fig. 1(b). It is clear that the As XMCD intensity correlates strongly with *T*c.

By applying the *s* ($l = 0$) core level orbital magnetization sum rule [25–27], the integrated XAS and XMCD intensities can be related to the element- and shell-selective orbital magnetic moment. For the *K* edge, the $4p$ orbital moment per hole is given by

$$\frac{\int_{E_f}^{E_c} dE[\mu^+(E) - \mu^-(E)]}{\int_{E_f}^{E_c} dE[\mu^+(E) + \mu^0(E) + \mu^-(E)]} = -\frac{\langle L_z \rangle_p}{n_p^h}, \quad (1)$$

where n_p^h is the number of holes in the p valence shell, and $\langle L_z \rangle_p$ is the p-projected ground state orbital magnetic moment. The transition from a $1s$ core to the continuum states of an isolated As ion was modeled by an arctan function and subtracted from the normalized isotropic, μ^0,

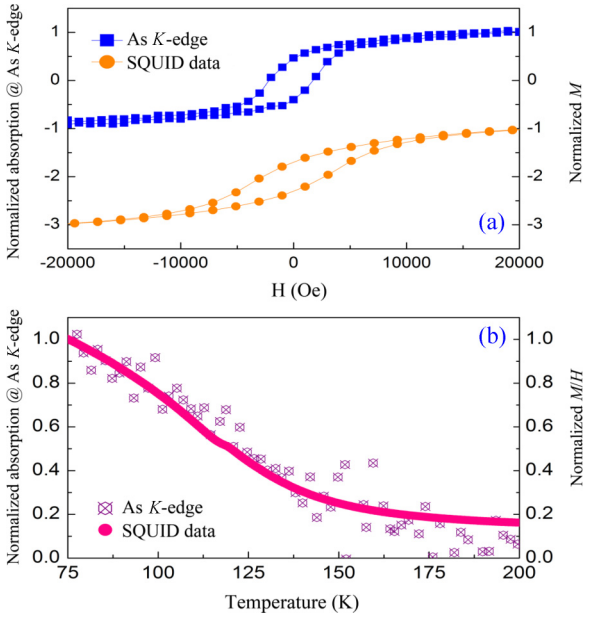

FIG. 2. (a) As K-edge hysteresis loops at $T = 2\,\mathrm{K}$, $P = 1$ bar for $(Ba_{0.75}K_{0.25})(Zn_{0.95}Mn_{0.05})_2As_2$. Orange solid circles (shifted by 2) show the sample hysteresis measured by SQUID magnetometry. (b) Temperature dependence of As K-edge XMCD (points) and SQUID data (solid line). SQUID data were obtained after zero field cooling, in $H = 500\,\mathrm{Oe}$. All data are normalized to unity at the highest magnetic field or lowest temperature. The SQUID data were collected on the same sample used in the XMCD measurements.

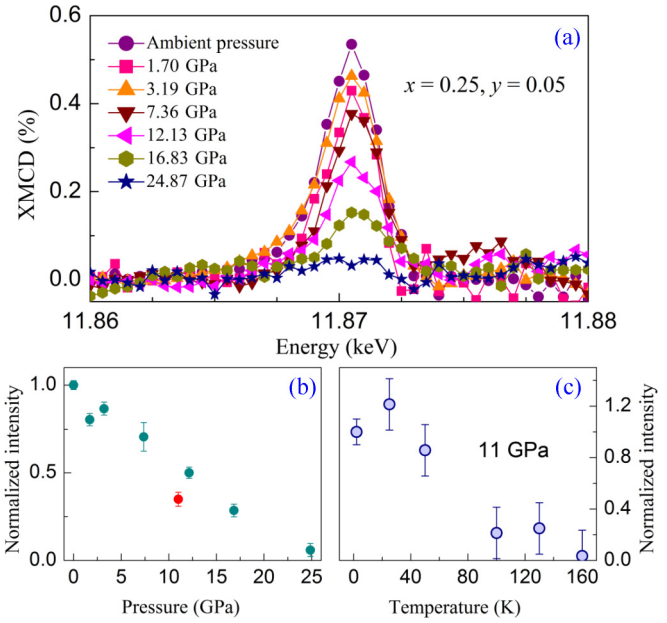

FIG. 3. (a) Pressure-dependent As K-edge XMCD signal for $(Ba_{0.75}K_{0.25})(Zn_{0.95}Mn_{0.05})_2As_2$. (b) XMCD peak intensity normalized to unity at $P = 1$ bar. Green data points are compression data, while the red data point was obtained on decompression. (c) Temperature-dependent As K-edge XMCD signal (taken after decompression to 11 GPa), normalized to its $T = 2\,\mathrm{K}$ value.

XAS data before the integration. For the $x = 0.25$, $y = 0.05$ sample at ambient pressure, taking $n_p^h = 0.125\,\mathrm{hole/As}$, we determined the value of the orbital moment in the As $4p$ band to be $\langle L_z \rangle_p = -0.000106(8)$. The As $4p$ spin polarization (due to $p-d$ hybridization) together with the spin-orbit interaction give rise to the orbital polarization in the $4p$ band, which is antiparallel to the net magnetization (dominated by Mn). Theoretical calculations [11] show that As atoms acquire spin polarization that is opposite to Mn polarization. We conclude that As spin and orbital moments are parallel and opposite to the Mn magnetic moments. The orbital magnetic moment per As ion obtained from sum-rule analysis shows an approximately linear relationship with increasing Tc [Fig. 1(c)]. The doping-dependent measurements indicate that the As orbital moment (polarization of charge carriers) is involved in mediating magnetic ordering.

To confirm that the As K-edge XMCD signal scales with the sample magnetization (dominated by Mn), we measured the external magnetic field- and temperature-dependent XMCD on the $x = 0.25$, $y = 0.05$ sample at ambient pressure. The XMCD closely follows the total magnetization measured by superconducting quantum interference device (SQUID) magnetometry and hence is strongly connected with the magnetic ordering of the bulk sample. The hysteresis and temperature-dependent XMCD data taken at the As K-edge, along with the M-H plot and zero-field-cooled M-T plot from SQUID are shown in Fig. 2. The XMCD signal was measured at a fixed energy $E = 11{,}870.5\,\mathrm{eV}$ corresponding to the XMCD peak position. The agreement in coercivity and Tc is robust, indicating that the As K-edge XMCD is representative of the bulk magnetization. These results further prove that the polarized As moments are induced by proximity to the magnetically ordered Mn ions in the $(Ba_{1-x}K_x)(Zn_{1-y}Mn_y)_2As_2$ system. This validates the conclusions in Ref. [11] and Ref. [28] and supports the model of carrier-mediated ferromagnetic ordering involving As-derived valence-band states.

Figure 3(a) shows the high-pressure As XMCD spectra taken at $T = 2\,\mathrm{K}$ and magnetic field of 2 T for the $x = 0.25$, $y = 0.05$ sample. The overall intensity of the spectra diminishes as the pressure increases, and only a remnant feature remains at 25 GPa. The relative XMCD peak intensities ($E = 11{,}870.5\,\mathrm{eV}$) measured on compression and decompression are plotted in Fig. 3(b). The pressure-induced quenching of the As XMCD signal is reversible. When decompressed to ~11 GPa, the signal returns to a value close to that observed on compression. As discussed above, the polarization of the As p band is strongly correlated with Tc, namely, the strength of ferromagnetic coupling between Mn atoms. Generally, the source of this indirect exchange interaction can be described as [29,30]: (i) a charge carrier is polarized by the p-d exchange interaction with a Mn^{2+} ion at a given site, and (ii) propagation of the polarized charge carrier mediates the interaction with a Mn^{2+} ion at another site. Therefore, the decrease of As XMCD intensity under pressure indicates the weakening of the ferromagnetic exchange between Mn ions. To directly verify this conclusion, we measured the temperature dependence of As XMCD at the decompressed pressure of 11 GPa [Fig. 3(c)], where the XMCD intensity is reduced by about a factor of 2 from its ambient-pressure value [Fig. 3(b)]. As expected, the ordering temperature decreases significantly. The onset

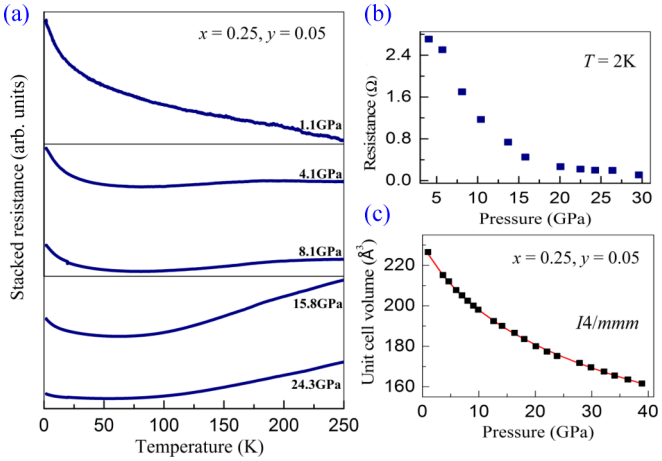

FIG. 4. (a) Temperature-dependent resistance plots at selected pressures for $(Ba_{0.75}K_{0.25})(Zn_{0.95}Mn_{0.05})_2As_2$. (b) Pressure-dependent sample resistance at fixed temperature of $T = 2$ K. (c) Unit cell volume under pressure for $(Ba_{0.75}K_{0.25})(Zn_{0.95}Mn_{0.05})_2As_2$. Solid black symbols represent experimental data, and the red line is a fit to a third-order Birch-Murnaghan equation of state.

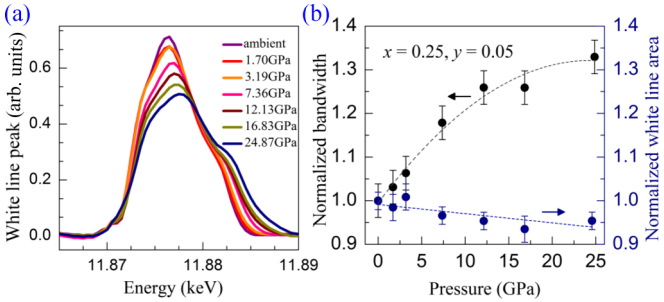

FIG. 5. (a) Background-subtracted "white line" peaks in As K-edge data at $T = 2$ K under different pressures for $(Ba_{0.75}K_{0.25})(Zn_{0.95}Mn_{0.05})_2As_2$. (b) Black solid points indicate white line peak width (bandwidth) under pressure, and blue solid points are the integrated area (number of holes) with pressure; all data are normalized to their $P = 1$ bar values. Dashed lines are guides to the eye.

temperature of magnetic order takes place at about 100 K, compared to 150 K at ambient pressure [Fig. 2(b)].

We also studied the pressure effect on the electrical transport properties of the $x = 0.25$, $y = 0.05$ sample. Technical details for these measurements can be found in Ref. [31]. The sample undergoes a semiconductor to metal-like transition upon compression, as shown in Fig. 4(a). The zero-field resistance measured at $T = 2$ K as a function of pressure is plotted in Fig. 4(b). The resistivity rapidly decreases with pressure, and an increase of more than one order of magnitude in conductivity is observed at 24 GPa. Since changes in crystal symmetry with pressure could dramatically influence the electronic degrees of freedom, we conducted *in-situ* high-pressure x-ray diffraction (XRD) experiments at the 16 BM-D beamline of the Advanced Photon Source at Argonne National Laboratory ($T = 300$ K). Rietveld refinements of the high-pressure data were performed with the GSAS package [32,33]. The $(Ba_{1-x}K_x)(Zn_{1-y}Mn_y)_2As_2$ DMS materials crystallize into a tetragonal $ThCr_2Si_2$-type structure (space group $I4/mmm$) at ambient pressure [7]. We found no structural phase transitions to 40 GPa, indicating that the suppression of magnetic order and concomitant emergence of a metal-like state under pressure are not a result of change in lattice symmetry (see Fig. S1 in the Supplemental Material [34]). Figure 4(c) shows that the unit cell volume is reduced by 23% at 24 GPa (bulk modulus $B = 45$ GPa). The compression of the lattice increases electronic bandwidth and enhances carrier mobility, as clearly seen in the transport measurements. The pressure experiments show that ferromagnetism and carrier mobility are strongly correlated. The spin polarization of hole carriers decreases as they become more itinerant, indicating that carrier mobility is intimately connected to the mechanism behind ferromagnetic ordering. Similar behavior was also observed in some high-temperature, weakly ferromagnetic iridate systems (see Ref. [35]). The electronic structure and magnetism are closely coupled to the lattice volume, which affects electronic bandwidth, hole mobility, and the strength of magnetic (exchange) interactions.

We now examine the XAS data in order to characterize the evolution of the As $4p$ band under pressure. Figure 5(a) displays the pressure-dependent "white lines" [shadowed area in Fig. 1(a)] obtained after subtracting the continuum (edge-step) contributions to the isotropic XAS ($T = 2$ K) spectra. Under compression, a gradual broadening of the $4p$ band is observed. The bandwidth is 33% larger at 25 GPa relative to ambient pressure, while the change of integrated area is only a few percent [Fig. 5(b)]. This indicates that the number of holes does not change significantly with pressure while hole mobility (bandwidth) does. These results show that bands derived from outer-shell $4p$ orbitals are quite compressible and that lattice compression alone can precipitate drastic changes in the ground state, namely, a semiconductor to metal-like transition accompanied by loss of ferromagnetic order. We conclude that the magnetic ordering of these materials is critically linked to the mobility of doped carriers. The pressure experiments are unique in that they allow isolation of the effect of hole mobility (bandwidth) on the exchange mechanism at fixed doping. This is of course impossible to achieve in doping experiments, where dopants add holes but also disorder, in addition to changes in bandwidth. It is worth noticing that even the highest achievable doping levels ($x = 0.3$) result in a semiconducting state at ambient pressure [7].

III. CONCLUSION

In summary, we have studied the induced polarization of doped As $4p$ carriers in the $(Ba_{1-x}K_x)(Zn_{1-y}Mn_y)_2As_2$ DMS system using XMCD under ambient- and high-pressure conditions. We find that this induced polarization scales with Tc; namely, it is a requirement for magnetic order of Mn ions. Second, we show that this induced carrier polarization is tied to carrier mobility: Magnetic order is lost when the system enters a nearly metallic state at about 25 GPa. Carrier (hole) mobility and polarization are intimately connected to the mechanism behind ferromagnetic ordering in this class of materials, and therefore their magnetic and transport properties can be readily modified with lattice compression.

ACKNOWLEDGMENTS

We thank Y. Ding, K. Liu, H. C. Yang, and Z. Y. Lu for helpful discussions. Gas loading by S. Tkachev is acknowledged. Work at APS was supported by the U.S. Department of Energy (DOE), Office of Science, under Contract No. DE-AC02-06CH11357. Work at Institute of Physics Chinese Academy of Sciences (Grants No. 11220101003, No. 11534016, and No. 112111KYS820150017) is supported by NSF, Ministry of Science & Technology, and Chinese Academy of Sciences of China through Research Projects. Work at HPSTAR is supported by the National Natural Science Foundation of China under Grants No. 51527801 and No. U1530402. H.K.M and W.Y. acknowledge financial support from the DOE-BES X-ray Scattering Core Program under Grant No. DE-FG02-99ER45775. The High Pressure Collaborative Access Team operations are supported by DOE-NNSA under Award No. DE-NA0001974 and DOE-BES under Award No. DE-FG02-99ER45775, with partial instrumentation funding by the National Science Foundation.

[1] H. Ohno, A. Shen, F. Matsukura, A. Oiwa, A. Endo, S. Katsumoto, and Y. Iye, Appl. Phys. Lett. **69**, 363 (1996).

[2] H. Ohno, Science **281**, 951 (1998).

[3] I. Zutic, J. Fabian, and D. Sarma, Rev. Mod. Phys. **76**, 323 (2004).

[4] T. Dietl, Nat. Mater. **9**, 965 (2010).

[5] T. Dietl, and H. Ohno, Rev. Mod. Phys. **86**, 187 (2014).

[6] Z. Deng, C. Q. Jin, Q. Q. Liu, X. C. Wang, J. L. Zhu, S. M. Feng, L. C. Chen, R. C. Yu, C. Arguello, T. Goko, F. Ning, J. Zhang, Y. Wang, A. A. Aczel, T. Munsie, T. J. Williams, G. M. Luke, T. Kakeshita, S. Uchida, W. Higemoto *et al.*, Nat. Commun. **2**, 422 (2011).

[7] K. Zhao, Z. Deng, X. C. Wang, W. Han, J. L. Zhu, X. Li, Q. Q. Liu, R. C. Yu, T. Goko, B. Frandsen, L. Liu, F. Ning, Y. J. Uemura, H. Dabkowska, G. M. Luke, H. Luetkens, E. Morenzoni, S. R. Dunsiger, A. Senyshyn, P. Böni *et al.*, Nat. Commun. **4**, 1442 (2013).

[8] K. Zhao, B. Chen, G. Q. Zhao, X. Li, Z. Yuan, Z. Deng, Q. Q. Liu, and C. Q. Jin, Chin. Sci. Bull. **59**, 2524 (2014).

[9] L. Chen, X. Yang, F. Yang, J. Zhao, J. Misuraca, P. Xiong, and S. Molnár, Nano Lett. **11**, 2584 (2011).

[10] N. Gonzalez Szwacki, J. A. Majewski, and T. Dietl, Phys. Rev. B **91**, 184409 (2015).

[11] J. K. Glasbrenner, I. Žutić, and I. I. Mazin, Phys. Rev. B **90**, 140403(R) (2014).

[12] B. Beschoten, P. A. Crowell, I. Malajovich, D. D. Awschalom, F. Matsukura, A. Shen, and H. Ohno, Phys. Rev. Lett. **83**, 3073 (1999).

[13] D. J. Keavney, D. Wu, J. W. Freeland, E. Johnston-Halperin, D. D. Awschalom, and J. Shi, Phys. Rev. Lett. **91**, 187203 (2003).

[14] V. Iota, J. P. Klepeis, C. Yoo, J. Lang, D. Haskel, and G. Srajer, Appl. Phys. Lett. **90**, 042505 (2007).

[15] N. Ishimatsu, H. Maruyama, N. Kawamura, M. Suzuki, Y. Ohishi, and O. Shimomura, J. Phys. Soc. Jpn. **76**, 064703 (2007).

[16] R. Torchio, Y. O. Kvashnin, S. Pascarelli, O. Mathon, C. Marini, L. Genovese, P. Bruno, G. Garbarino, A. Dewaele, F. Occelli, and P. Loubeyre, Phys. Rev. Lett. **107**, 237202 (2011).

[17] E. Duman, M. Acet, E. F. Wassermann, J. P. Itie, F. Baudelet, O. Mathon, and S. Pascarelli, Phys. Rev. Lett. **94**, 075502 (2005).

[18] D. Haskel, G. Fabbris, N. M. Souza-Neto, M. van Veenendaal, G. Shen, A. E. Smith, and M. A. Subramanian, Phys. Rev. B **84**, 100403(R) (2011).

[19] S. Stahler, G. Schutz, and H. Ebert, Phys. Rev. B **47**, 818 (1993).

[20] I. Harada, and A. Kotani, J. Phys. Soc. Jpn. **63**, 1285 (1994).

[21] J. I. Igarashi, and K. Hirai, Phys. Rev. B **50**, 17820 (1994).

[22] A. A. Freeman, K. W. Edmonds, G. van der Laan, R. P. Campion, A. W. Rushforth, N. R. S. Farley, T. K. Johal, C. T. Foxon, B. L. Gallagher, A. Rogalev, and F. Wilhelm, Phys. Rev. B **77**, 073304 (2008).

[23] P. Wadley, A. A. Freeman, K. W. Edmonds, G. van der Laan, J. S. Chauhan, R. P. Campion, A. W. Rushforth, B. L. Gallagher, C. T. Foxon, F. Wilhelm, A. G. Smekhova, and A. Rogalev, Phys. Rev. B **81**, 235208 (2010).

[24] B. G. Ueland, Abhishek Pandey, Y. Lee, A. Sapkota, Y. Choi, D. Haskel, R. A. Rosenberg, J. C. Lang, B. N. Harmon, D. C. Johnston, A. Kreyssig, and A. I. Goldman, Phys. Rev. Lett. **114**, 217001 (2015).

[25] B. T. Thole, P. Carra, F. Sette, and G. van der Laan, Phys. Rev. Lett. **68**, 1943 (1992).

[26] P. Carra, B. T. Thole, M. Altarelli, and X. D. Wang, Phys. Rev. Lett. **70**, 694 (1993).

[27] G. Y. Guo, J. Phys.: Condens. Matter **8**, L747 (1996).

[28] H. Suzuki, K. Zhao, G. Shibata, Y. Takahashi, S. Sakamoto, K. Yoshimatsu, B. J. Chen, H. Kumigashira, F.-H. Chang, H.-J. Lin, D. J. Huang, C. T. Chen, Bo Gu, S. Maekawa, Y. J. Uemura, C. Q. Jin, and A. Fujimori, Phys. Rev. B **91**, 140401(R) (2015).

[29] M. Csontos, G. Mihály, B. Jankó, T. Wojtowicz, X. Liu, and J. K. Furdyna, Nat. Mater. **4**, 447 (2005).

[30] T. Jungwirth, Jairo Sinova, J. Mašek, J. Kučera, and A. H. MacDonald, Rev. Mod. Phys. **78**, 809 (2006).

[31] P. P. Kong, F. Sun, L. Y. Xing, J. Zhu, S. J. Zhang, W. M. Li, Q. Q. Liu, X. C. Wang, S. M. Feng, X. H. Yu, L. Zhu, R. C. Yu, W. G. Yang, G. Y. Shen, Y. S. Zhao, R. Ahuja, H. K. Mao, and C. Q. Jin, Sci. Rep. **4**, 6679 (2014).

[32] A. C. Larson and R. B. V. Dreele, Los Alamos National Laboratory Report No. LAUR 86, 2004.

[33] L. W. Finger, D. E. Cox, and A. P. Jephcoat, J. Appl. Crystallogr. **20**, 79 (1987).

[34] See Supplemental Material at http://link.aps.org/supplemental/10.1103/PhysRevB.93.224403 for the details of the high-pressure XRD measurements and diffraction patterns at selected pressures.

[35] G. Cao, X. N. Lin, S. Chikara, V. Durairaj, and E. Elhami, Phys. Rev. B **69**, 174418 (2004).